CHEMISTRY OF MATERIALS

Article

From Isolated Ag Ions to Aggregated Ag Nanoclusters in Silver-Exchanged Engelhard Titanosilicate (ETS-10) Molecular Sieve: Reversible Behavior

G. Agostini, S. Usseglio, E. Groppo, M. J. Uddin, C. Prestipino, S. Bordiga, A. Zecchina, P. L. Solari, and C. Lamberti

Chem. Mater., **2009**, 21 (7), 1343-1353• DOI: 10.1021/cm803216k • Publication Date (Web): 13 March 2009

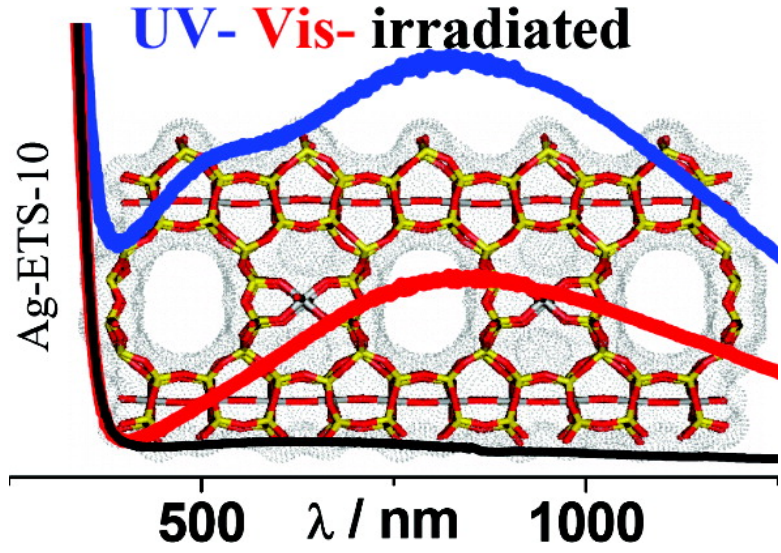

More About This Article

Additional resources and features associated with this article are available within the HTML version:

- Supporting Information
- Access to high resolution figures
- Links to articles and content related to this article
- Copyright permission to reproduce figures and/or text from this article

View the Full Text HTML

From Isolated Ag^+ Ions to Aggregated Ag^0 Nanoclusters in Silver-Exchanged Engelhard Titanosilicate (ETS-10) Molecular Sieve: Reversible Behavior

G. Agostini,[†] S. Usseglio,[†,‡] E. Groppo,[†] M. J. Uddin,[†] C. Prestipino,[§] S. Bordiga,[†] A. Zecchina,[†] P. L. Solari,[||] and C. Lamberti*,[†]

Department of Inorganic, Materials and Physical Chemistry, Torino University, Via P. Giuria 7, I-10125 Turin, Italy, INSTM Unità di Torino Università, Turin, Italy, NIS Centre of Excellence, Università di Torino, Italy, ESRF, 6 rue Jules Horowitz, BP220, F-38043, Grenoble Cedex, France, Synchrotron SOLEIL, L'Orme des Merisiers, Saint-Aubin, BP48, F-91192 Gif sur Yvette Cedex, France

Received November 28, 2008. Revised Manuscript Received January 14, 2009

Recently, it has been shown that Engelhard titanosilicate (ETS-10), a crystalline microporous titanosilicate, is an inverse-shape-selective photocatalyst. The main drawback in the extensive use of this material was its band gap value, located in the UV, that does not allow the use of solar light. In this work, we succeed in shifting the ETS-10 light absorption down to the visible region of the electromagnetic spectrum by introducing Ag^+ cations inside the ETS-10 channels. Thermal-, chemical-, and UV-phototreatments have been applied to Ag−ETS-10 to tune, in a controlled and progressive way, the aggregation of isolated Ag^+ counterions into metal nanoclusters of increasing nuclearity. This is a direct means to tune the frequency of silver nanoparticle plasmon resonance and thus the light absorption properties of the material. It is further reported that transformation of isolated Ag^+ ions into aggregated Ag^0 nanoclusters is almost reversible. Cycles of H_2-chemical reduction/O_2-chemical oxidation and of UV-photoreduction/vis-photo-oxidation are reported. UV−vis, Ag K-edge extended X-ray absorption fine structure (EXAFS), and Fourier transform infrared (FTIR) spectroscopy of adsorbed CO are the main techniques used to monitor the evolution of the silver aggregation along the different reduction/oxidation treatments.

1. Introduction

Engelhard titanosilicate (ETS-10) is a microporous crystalline material belonging to the family of Ti substituted silicates containing Ti in octahedral coordination.[1,2] Because of its inherently disordered nature, showing the presence of different polymorphs, conventional diffraction approaches could not be applied and the structure of ETS-10 was solved only five years after its synthesis by Anderson et al.,[3−5] combining an impressive number of complementary experimental techniques with molecular modeling simulations. They proved that the ETS-10 framework is composed of corner-sharing SiO_4 tetrahedra and TiO_6 octahedra linked through bridging oxygen atoms and that two sets of perpendicular 12-ring channels having an elliptical cross-section with dimension 7.6 Å × 4.9 Å are present. TiO_6 octahedra form linear −Ti−O−Ti−O−Ti− chains running along both *a* and *b* directions, as represented in Figure 1a. Validation of this model came successively by different groups using different approaches, among which we recall: (i) the single-crystal X-ray diffraction (XRD) study performed by Wang and Jacobson,[6] which has been able to grow and isolate a single crystal formed by an unique polymorph, (ii) the periodic density functional theory (DFT) study by Damin et al.,[7] and (iii) the Ti K-edge extended X-ray absorption fine structure (EXAFS) study by Prestipino et al.[8]

The insertion of a Ti(IV) atom in a 6-fold coordinated framework site implies the transfer of two electrons to the lattice which becomes negatively charged. The resulting negative charge of the framework $[Si_{40}Ti_8O_{104}]^{16-}$ unit is balanced by the presence of Na^+ and K^+ counterions located in the channels,[6,9−13] as reported in Figure 1b. The high number of framework Ti (Si/Ti = 5) and the fact that each Ti needs the presence of two monovalent counterions make the number of counterions rather high. This fact implies that

* Corresponding author. Tel.: +39011-6707841. Fax: +390116707855. E-mail: carlo.lamberti@unito.it.
[†] Department of Chemistry and NIS Torino University.
[‡] Present address: SINTEF Materials and Chemistry, Postboks 124, Blindern, N-0314, Oslo, Norway.
[§] ESRF.
[||] SOLEIL.

(1) Kuznicki, S. M. U.S. Patent 438939, 1990.
(2) Kuznicki, S. M.; Thrush, K. A.; Allen, F. M.; Levine, S. M.; Hamil, M. M.; Hayhurst, D. T.; Mansour, M. Synthesis and adsorpitive Properties of Titanium Silicate Molecular Sieves. In *Synthesis of Microporous Materials*; Ocelli, M. L., Robson, H. E., Ed.; Van Nostrand Reinhold: New York, 1992; Vol. 1, p 427.
(3) Anderson, M. W.; Terasaki, O.; Ohsuna, T.; Philippou, A.; Mackay, S. P.; Ferreira, A.; Rocha, J.; Lidin, S. *Nature* **1994**, *367*, 347–351.
(4) Anderson, M. W.; Terasaki, O.; Ohsuna, T.; Malley, P. J. O.; Philippou, A.; Mackay, S. P.; Ferreira, A.; Rocha, J.; Lidin, S. *Philos. Mag. B* **1995**, *71*, 813–841.
(5) Ohsuna, T.; Terasaki, O.; Watanabe, D.; Anderson, M. W.; Lidin, S. *Stud. Surf. Sci. Catal.* **1994**, *84*, 413–420.
(6) Wang, X. Q.; Jacobson, A. J. *Chem. Commun.* **1999**, 973–974.
(7) Damin, A.; Llabrés i Xamena, F. X.; Lamberti, C.; Civalleri, B.; Zicovich-Wilson, C. M.; Zecchina, A *J. Phys. Chem. B* **2004**, *108*, 1328–1336.
(8) Prestipino, C.; Solari, P. L.; Lamberti, C. *J. Phys. Chem. B* **2005**, *109*, 13132–13137.
(9) Grillo, M. E.; Carrazza, J. *J. Phys. Chem. B* **1997**, *101*, 6749–6752.

10.1021/cm803216k CCC: $40.75
Published on Web 03/13/2009

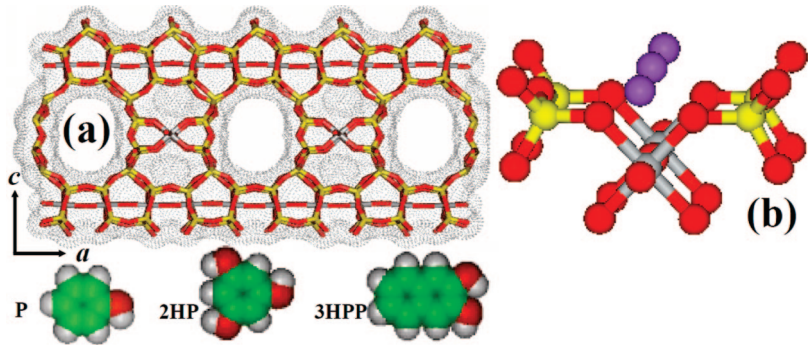

Figure 1. (a) Stick representation of ETS-10 structure viewed along the *b* direction. Si, Ti, and O atoms are represented as yellow, gray, and red sticks, respectively. For sake of clarity, charge-balancing cations have been omitted. −Ti−O−Ti−O−Ti− chains, running along the *a* and *b* directions, are visible. The available free space in the channels running along the *b* direction is evidenced using the Connolly algorithm. Among the three different aromatic molecules reported below, only phenol (P) is able to penetrate inside the ETS-10 channels. (b) Stick and ball representation, zoomed in on a fraction of the −Ti−O−Ti−O−Ti− chain showing also the charge-balancing monovalaent cations (violet balls). The other colors are as described in part a.

ETS-10 is a microporous material exhibiting remarkable cation exchange capabilities. It has been shown that alkali−metal cations can easily substitute the original Na^+ and K^+ counterions leading to the Li^+, Na^+, K^+, Rb^+, or Cs^+ forms.[13−15] Cation exchange with NH_4^+ results in the preparation of H−ETS-10, a microporous titanosilicate with Brønsted acidity.[13,16,17] Also divalent cations like platinum,[18,19] strontium,[20] magnesium,[21,22] and copper[23] have been successfully introduced as counterions inside the ETS-10 framework.

As mentioned above, the most interesting structural peculiarity of ETS-10 consists in the presence of linear chains of TiO_6 octahedra forming −Ti−O−Ti−O−Ti− quantum wires embedded in an highly insulating SiO_2 matrix. Consequently, ETS-10 exhibits a semiconducting character with an energy gap blue-shifted by about 1 eV with respect to bulk TiO_2,[24,25] due to quantum confinement effects.[14,26] Periodic one-dimensional ab initio calculations confirmed this interpretation.[7,27] This semiconductor peculiarity makes ETS-10 a material able to photodegradate aromatic pollutants hosted at the pore opening of the particles, where surface Ti−OH groups appear. Smaller molecules (like phenol) that can penetrate inside the channels (see molecules sketched in the bottom part of Figure 1a) are prevented from photodegradation owing to the absence of active titanol groups. Consequently, the combination of microporous structure with semiconductor electronic behavior makes ETS-10 an interesting material in the field of photocatalysis, because of its "inverse shape selectivity".[16,28−32] In particular, molecules of different steric hindrance like phenol (P), 1,3,5-trihydroxybenzene (3HP) and 2,3-dihydroxynaphthalene (2HPP), see Figure 1a, have been photodegraded inside ETS-10 according to the following rate P ≪ 3HP < 2HPP.[28,30]

However, until now, these elegant findings lie on academic ground only, because the quantum confinement shifts the band gap in the opposite direction with respect to what is needed to exploit a large fraction of the solar spectrum. UV-radiation, expensive for a large scale application, is needed to make the ETS-10 work,[28,30] and only in few lucky cases do the HOMO−LUMO levels of the adsorbed molecule properly match that of the semiconductor conduction band to allow a dye-sensitized process to be operative.[32] Recently, the group of Garcia and Corma has been able to realize active solar cells by incorporating a ruthenium polypyridyl dye inside ETS-10 channels.[33]

(10) Ganapathy, S.; Das, T. K.; Vetrivel, R.; Ray, S. S.; Sen, T.; Sivasanker, S.; Delevoye, L.; Fernandez, C.; Amoureux, J. P. *J. Am. Chem. Soc.* **1998**, *120*, 4752–4762.
(11) Anderson, M. W.; Agger, J. R.; Luigi, D. P.; Baggaley, A. K.; Rocha, J. *Phys. Chem. Chem. Phys.* **1999**, *1*, 2287–2292.
(12) Rocha, J.; Anderson, M. W. *Eur. J. Inorg. Chem.* **2000**, *80*, 1–818.
(13) Zecchina, A.; Llabrés i Xamena, F. X.; Pazé, C.; Turnes Palomino, G.; Bordiga, S.; Otero Areán, C *Phys. Chem. Chem. Phys.* **2001**, *3*, 1228–1231.
(14) Lamberti, C. *Microporous Mesoporous Mater.* **1999**, *30*, 155–163.
(15) Anson, A.; Wang, Y.; Lin, C. C. H.; Kuznicki, T. M.; Kuznicki, S. M. *Chem. Eng. Sci.* **2008**, *63*, 4171–4175.
(16) Howe, R. F.; Krisnandi, Y. K. *Chem. Commun.* **2001**, 1588–1589.
(17) Krisnandi, Y. K.; Lachowski, E. E.; Howe, R. F. *Chem. Mater.* **2006**, *18*, 928–933.
(18) Philippou, A.; Naderi, M.; Pervaiz, N.; Rocha, J.; Anderson, M. W. *J. Catal.* **1998**, *178*, 174–181.
(19) Waghmode, S. B.; Das, T. K.; Vetrivel, R.; Sivasanker, S. *J. Catal.* **1999**, *185*, 265–271.
(20) Braunbarth, C.; Hillhouse, H. W.; Tsapatsis, M.; Burton, A.; Lobo, R. F.; Jacubinas, R. M.; Kuznicki, S. M. *Chem. Mater.* **2000**, *12*, 1857–1865.
(21) Otero Areán, C.; Turnes Palomino, G.; Zecchina, A.; Bordiga, S.; Llabrés i Xamena, F. X.; Pazé, C *Catal. Lett.* **2000**, *66*, 231–235.
(22) Llabrés i Xamena, F. X.; Zecchina, A *Phys. Chem. Chem. Phys.* **2002**, *4*, 1978–1982.
(23) Bordiga, S.; Pazé, C.; Berlier, G.; Scarano, D.; Spoto, G.; Zecchina, A.; Lamberti, C. *Catal. Today* **2001**, *70*, 91–105.
(24) Carp, O.; Huisman, C. L.; Reller, A. *Prog. Solid State Chem.* **2004**, *32*, 33–177.
(25) Diebold, U. *Surf. Sci. Rep.* **2003**, *48*, 53–229.
(26) Borello, E.; Lamberti, C.; Bordiga, S.; Zecchina, A.; Otero Areán, C. *Appl. Phys. Lett.* **1997**, *71*, 2319–2321.
(27) Bordiga, S.; Turnes Palomino, G.; Zecchina, A.; Ranghino, G.; Giamello, E.; Lamberti, C. *J. Chem. Phys.* **2000**, *112*, 3859–3867.
(28) Calza, P.; Pazé, C.; Pelizzetti, E.; Zecchina, A. *Chem. Commun.* **2001**, 2130–2131.
(29) Southon, P. D.; Howe, R. F. *Chem. Mater.* **2002**, *14*, 4209–4218.
(30) Llabrés i Xamena, F. X.; Calza, P.; Lamberti, C.; Prestipino, C.; Damin, A.; Bordiga, S.; Pelizzetti, E.; Zecchina, A *J. Am. Chem. Soc.* **2003**, *125*, 2264–2271.
(31) Krisnandi, Y. K.; Howe, R. F. *Appl. Catal. A: Gen.* **2006**, *307*, 62–69.
(32) Usseglio, S.; Calza, P.; Damin, A.; Minero, C.; Bordiga, S.; Lamberti, C.; Pelizzetti, E.; Zecchina, A. *Chem. Mater.* **2006**, *18*, 3412–3424.
(33) Atienzar, P.; Valencia, S.; Corma, A.; Garcia, H. *ChemPhysChem* **2007**, *8*, 1115–1119.
(34) Anson, A.; Kuznicki, S. M.; Kuznicki, T.; Haastrup, T.; Wang, Y.; Lin, C. C. H.; Sawada, J. A.; Eyring, E. M.; Hunter, D. *Microporous Mesoporous Mater.* **2008**, *109*, 577–580.
(35) Kuznicki, S. M.; Anson, A.; Koenig, A.; Kuznicki, T. M.; Haastrup, T.; Eyring, E. M.; Hunter, D. *J. Phys. Chem. C* **2007**, *111*, 1560–1562.

Here, we report an attempt to shift the ETS-10 light absorption down to the visible region of the electromagnetic spectrum. The work consists of the preparation of a silver-exchanged ETS-10[15,34,35] and, in the consequent thermal-, chemical-, and phototreatments aimed to tune, in a controlled and progressive way, the reduction and the aggregation of isolated Ag^+ counterions into metal clusters of increasing nuclearity. It is in fact known that silver nanoclusters exhibit a plasmon resonance[36−38] that absorbs in the visible and that Ag-doped TiO_2 materials have been already exploited to improve the photoactivity of titania with solar light.[39−44] The reduction/oxidation chemistry of the silver in ETS-10 has been followed mainly by UV−vis and Ag K-edge EXAFS spectroscopies, supported by infrared (IR) spectroscopy. Such a multitechnical characterization approach is particularly important when complex systems, like Ag−ETS-10, are investigated.

On top of this, Ag ion-exchanged zeolites have attracted special attention, since they are photochemically active and induce various photocatalytic and photochemical reactions. Isolated Ag^+ ions, as well as small Ag ion clusters, can be stabilized within the nanoscaled pore systems of zeolites and play a significant role in the photocatalytic and photochemical reactions as the active or electron-trapping site.[45−56] Consequently, the ability to tune the silver nucleation inside porous solids is highly demanded.

2. Experimental Details

The Na−K−ETS-10 sample (Na/K = 2.64, hereafter ETS-10), kindly supplied by Engelhard (Iselin, NJ), comes from the same batch already used by us for previous investigations.[7,8,14,26−28,30,57,58] The protonic form (hereafter H−ETS-10) has been obtained from ETS-10 by cation exchange with NH_4^+ and then calcined, as described elsewhere.[13] Ag−ETS-10 has been obtained by impregnating H−ETS-10 with a water solution of $AgNO_3$. The mixture was then stirred at room temperature (RT) for 1 h, filtered and washed with deionized water, and partially dried at RT under N_2 flow. Elemental analysis reveals a partial exchange level of 7.5 Ag wt % corresponding to a Ag/Ti ratio of 0.3.

H_2-reduced Ag−ETS-10 samples have been prepared in our laboratories according to the following protocol: activation in vacuum (10^{-4} Torr) at 373 K to remove most of the adsorbed water; (ii) temperature decrease in vacuo down to room temperature; (iii) dosage of H_2 (50 Torr); (iv) temperature increase in H_2 atmosphere up to the desired temperature. Reoxidized samples have been obtained by increasing the temperature in O_2 atmosphere up to the desired temperature.

Photoreduction has been obtained using a UV photon box (Polymer GN 400 ZS, Helios Italquartz, Italy) able to irradiate the sample, whose temperature is kept constant at 308 K, with a power of 50 mW/cm^2 for 15 min in air at atmospheric humidity. For photo-re-oxidation, the irradiation was carried out on the previously UV-reduced sample using a SOL2/500S lamp (honle UV technology, Munchen, Germany) simulating solar light. The SOL-bulb and the H_2 filter together yield a spectrum very similar to the natural sunlight, ranging from ultraviolet to infrared radiation (approx 295−3000 nm). Also in this case, the sample temperature was kept constant at 308 K, while the irradiation time was 24 h.

The powder XRD pattern has been collected on a Philips PW3020 X-ray diffractometer operating with Cu Kα radiation in a Bragg−Brentano configuration. The IR spectra were collected using a Bruker IFS66 spectrometer with a resolution of 2 cm^{-1}. The sample was pressed into a self-supporting pellet and inserted into an homemade quartz cell allowing thermal treatments and in situ measurements in controlled atmosphere and in the 100−800 K temperature range. UV−vis spectra have been collected in reflectance mode (DRS) with a Perkin-Elmer Lambda 19 spectrometer and reported using the Kubelka−Munk function. The sample was measured in the powdered form, inside a cell equipped with a cuvette of optical quartz, allowing treatments and measurements in controlled atmosphere.

X-ray absorption experiments on the Ag K-edge (25514 eV) have been performed at the BM29[59] beamline at the European Synchrotron Radiation Facility (ESRF, Grenoble, France). The monochromator was equipped with two Si(311) crystals; harmonic rejection was achieved by detuning at 30% of the maximum of the rocking curve. The following experimental geometry was adopted: (1) I_0 (25% efficiency); (2) sample; (3) I_1 (90% efficiency); (4) Ag foil reference sample; (5) I_2 (90% efficiency).[60] This setup allows a direct energy/angle calibration for each spectrum avoiding any problem related to little energy shifts due to small thermal instability of the monochromator crystals. For the X-ray absorption near-edge structure (XANES) part, a sampling step of 0.5 eV has been applied, while for the EXAFS part, a constant sampling step in k-space (Δk = 0.03 Å^{-1}) has been used. For each sampled point, an integration time of 3 s has been used. Spectra have been collected at RT in

(36) Evanoff, D. D.; Chumanov, G. *J. Phys. Chem. B* **2004**, *108*, 13957–13962.
(37) Kumbhar, A.; Chumanov, G. *J. Nanosci. Nanotechnol.* **2004**, *4*, 299–303.
(38) Evanoff, D. D.; Chumanov, G. *ChemPhysChem* **2005**, *6*, 1221–1231.
(39) Seery, M. K.; George, R.; Floris, P.; Pillai, S. C. *J. Photochem. Photobiol. A: Chem.* **2007**, *189*, 258–263.
(40) Andersson, M.; Birkedal, H.; Franklin, N. R.; Ostomel, T.; Boettcher, S.; Palmqvist, A. E. C.; Stucky, G. D. *Chem. Mater.* **2005**, *17*, 1409–1415.
(41) Ozkan, A.; Ozkan, M. H.; Gurkan, R.; Akcay, M.; Sokmen, M. *J. Photochem. Photobiol. A: Chem.* **2004**, *163*, 29–35.
(42) Zhang, F. X.; Guan, N. J.; Li, Y. Z.; Zhang, X.; Chen, J. X.; Zeng, H. S. *Langmuir* **2003**, *19*, 8230–8234.
(43) Sokmen, M.; Ozkan, A. *J. Photochem. Photobiol. A: Chem.* **2002**, *147*, 77–81.
(44) Uddin, M. J.; Cesano, F.; Bertarione, S.; Bonino, F.; Bordiga, S.; Scarano, D.; Zecchina, A. *J. Photochem. Photobiol. A: Chem.* **2008**, *196*, 165–173.
(45) Stein, A.; Ozin, G. A.; Macdonald, P. M.; Stucky, G. D.; Jelinek, R. *J. Am. Chem. Soc.* **1992**, *114*, 5171–5186.
(46) Stein, A.; Ozin, G. A.; Stucky, G. D. *J. Am. Chem. Soc.* **1992**, *114*, 8119–8129.
(47) Beer, R.; Binder, F.; Calzaferri, G. *J. Photochem. Photobiol. A: Chem.* **1992**, *69*, 67–72.
(48) Sun, T.; Seff, K. *Chem. Rev.* **1994**, *94*, 857–870.
(49) Matsuoka, M.; Matsuda, E.; Tsuji, K.; Yamashita, H.; Anpo, M. *J. Mol. Catal. A: Chem.* **1996**, *107*, 399–403.
(50) Anpo, M.; Zhang, S. G.; Mishima, H.; Matsuoka, M.; Yamashita, H. *Catal. Today* **1997**, *39*, 159–168.
(51) Szulbinski, W. S. *Inorg. Chim. Acta* **1998**, *269*, 253–259.
(52) Ju, W. S.; Matsuoka, M.; Iino, K.; Yamashita, H.; Anpo, M. *J. Phys. Chem. B* **2004**, *108*, 2128–2133.
(53) Calzaferri, G.; Leiggener, C.; Glaus, S.; Schurch, D.; Kuge, K. *Chem. Soc. Rev.* **2003**, *32*, 29–37.
(54) Matsuoka, M.; Anpo, M. *Curr. Opin. Solid State Mater. Sci.* **2003**, *7*, 451–459.
(55) Bruhwiler, D.; Calzaferri, G. *Microporous Mesoporous Mater.* **2004**, *72*, 1–23.
(56) Uma, S.; Rodrigues, S.; Martyanov, I. N.; Klabunde, K. J. *Microporous Mesoporous Mater.* **2004**, *67*, 181–187.
(57) Zecchina, A.; Otero Areán, C.; Turnes Palomino, G.; Geobaldo, F.; Lamberti, C.; Spoto, G.; Bordiga, S. *Phys. Chem. Chem. Phys.* **1999**, *1*, 1649–1657.
(58) Llabrés i Xamena, F. X.; Damin, A.; Bordiga, S.; Zecchina, A. *Chem. Commun.* **2003**, *151*, 4–1515.
(59) Filipponi, A.; Borowski, M.; Bowron, D. T.; Ansell, S.; Di Cicco, A.; De Panfilis, S.; Itie, J. P. *Rev. Sci. Instrum.* **2000**, *71*, 2422–2432.
(60) Lamberti, C.; Bordiga, S.; Bonino, F.; Prestipino, C.; Berlier, G.; Capello, L.; D'Acapito, F.; Llabrés i Xamena, F. X.; Zecchina, A *Phys. Chem. Chem. Phys.* **2003**, *5*, 4502–4509.

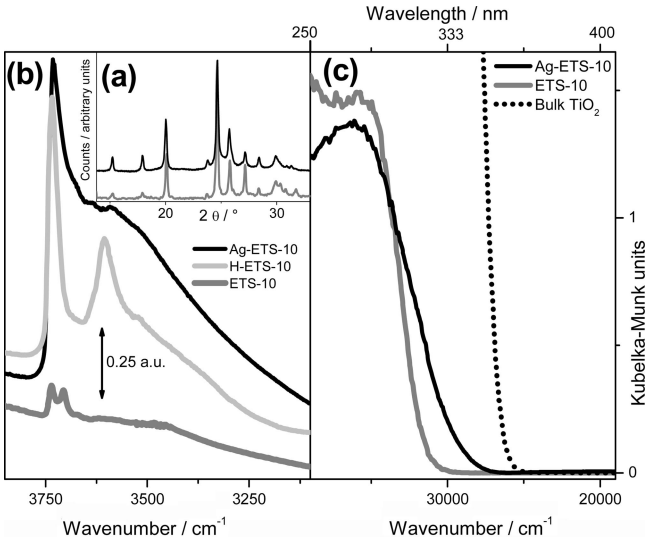

Figure 2. (a) Powder XRD patterns (Cu Kα radiation) of Ag−ETS-10 and ETS-10 (black and gray curves, respectively). (b) IR spectra in the O−H stretching region of Ag−ETS-10 (black), H−ETS-10 (light gray), and ETS-10 (dark gray, vertically rescaled for clarity): a.u. = absorbance units. (c) UV−vis DRS spectra of Ag−ETS-10 (full black curve) and ETS-10 (full gray curve). For comparison, also the spectrum of bulk TiO_2 is reported (dotted black curve).

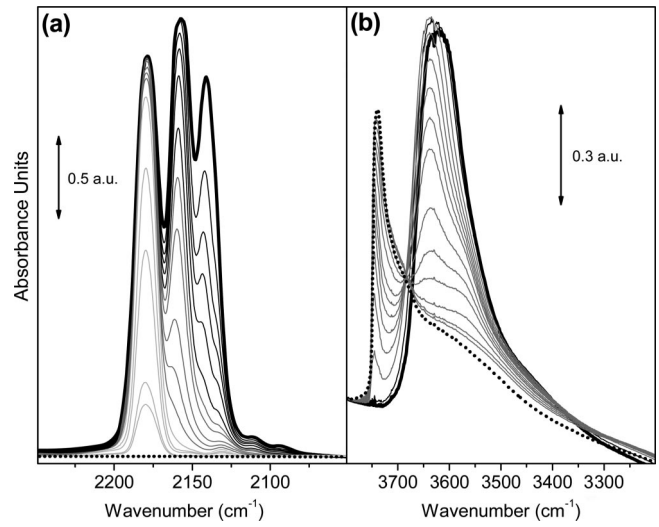

Figure 3. Evolution of IR spectra of CO adsorbed, at 100 K, on Ag−ETS-10 outgassed in a vacuum at 423 K down to 10^{-4} Torr (dotted black spectrum) upon increasing equilibrium pressure (up to $P_{CO} = 50$ Torr, black bold spectrum). The light gray spectra (not reported in part b) refer to the lowest P_{CO} (where only Ag^+ sites are engaged), and dark gray spectra refer to intermediate P_{CO} (where also O−H groups are engaged), while black curves refer to the highest P_{CO} values (where liquidlike CO is formed in the zeolitic cages). Part a reports background subtracted spectra and refers to the ν(CO) stretching region. Part b refers to the ν(OH) stretching region.

the 25 310−27 040 eV range, using a metallic cell allowing in situ high temperature treatments and gas dosage.[61] Extraction of the $\chi(k)$ functions and relative Fourier transforms (FTs) have been performed using the Athena and Arthemis codes.[62] To allow a direct comparison among all data, the k interval of the FT has been limited to 1.4−11.7 $Å^{-1}$, corresponding to the region of a good S/N ratio for the sample containing only isolated Ag^+ species. This choice has influence on the shape of the first shell Ag−Ag contribution that appears with two distinct maxima. Such k-interval dependent features of the modulus of the FT are typical of first shell scattering atoms with high Z numbers, as shown, e.g., for the As−In scattering,[63−65] (see the Supporting Information for a deeper discussion on this technical point, in particular Figure S1).

3. Characterization of the Ag-Exchanged Material

3.1. Framework Stability upon Ag^+ Exchange. Although only partial, the silver exchange causes a small degradation of the ETS-10 framework perfection, evidenced by the broadening of the reflections of the XRD pattern with respect to those of the parent ETS-10 material (compare black and gray curves in Figure 2a). Among all, note the multiplet around $2\theta = 30°$ that becomes a unique component tiled at the high 2θ side. The entity of the damage is however small, as the fingerprint pattern of the ETS-10 framework is very recognizable. Crystal damage results in the breaking of some Si−O−Si, Ti−O−Ti, and Si−O−Ti bonds, as testified by the IR study that showed, in the 3680−3200 cm^{-1} range (black curve in Figure 2b), the presence of H-bonded OH species of heterogeneous strength. Note that this broad IR component is very different from those observed in the ETS-10 and H−ETS-10 cases. ETS-10 (dark gray curve in Figure 2b) shows a well-defined doublet at 3735 and 3705 cm^{-1}, assigned to external silanols and titanols.[32] H−ETS-10 is characterized by a sharp peak at 3735 cm^{-1} due to the same species and by a band at 3600 cm^{-1} due to Brønsted Ti−OH−Si sites (see light gray curve in Figure 2b). The partial framework damage influences also the electronic properties of the material, as the absorption edge is no more as sharp as in the case of both TiO_2 bulk and parent ETS-10 (see Figure 2c).

3.2. Available Surface Sites Probed by IR Spectroscopy of Adsorbed CO. Among the methods for studying the surface properties of solids, FTIR spectroscopy of small adsorbed molecules (for instance CO) represents a very powerful tool.[66−69] In Figure 3, the FTIR spectra of CO adsorbed at 100 K on Ag−ETS-10 activated at 423 K (residual pressure 10^{-4} Torr) are reported as a function of increasing CO equilibrium pressure (P_{CO}). Parts a and b refer to the C−O and the O−H stretching regions, respectively. The activation temperature of 423 K has been chosen as a compromise to allow the almost complete water elimination without a significant Ag clustering effect (vide infra EXAFS

(61) Lamberti, C.; Prestipino, C.; Bordiga, S.; Berlier, G.; Spoto, G.; Zecchina, A.; Laloni, A.; La Manna, F.; D'Anca, F.; Felici, R.; D'Acapito, F.; Roy, P. *Nucl. Instrum. Methods Phys. Res. B* **2003**, *200*, 196–201.
(62) Ravel, B.; Newville, M. *J. Synchrot. Radiat.* **2005**, *12*, 537–541.
(63) Lamberti, C.; Bordiga, S.; Boscherini, F.; Pascarelli, S.; Schiavini, G. M. *Appl. Phys. Lett.* **1994**, *64*, 1430–1432.
(64) Lamberti, C.; Bordiga, S.; Boscherini, F.; Mobilio, S.; Pascarelli, S.; Gastaldi, L.; Madella, M.; Papuzza, C.; Rigo, C.; Soldani, D.; Ferrari, C.; Lazzarini, L.; Salviati, G. *J. Appl. Phys.* **1998**, *83*, 1058–1077.
(65) Pascarelli, S.; Boscherini, F.; Lamberti, C.; Mobilio, S. *Phys. Rev. B* **1997**, *56*, 1936–1947.
(66) Lercher, J. A.; Grundling, C.; EderMirth, G. *Catal. Today* **1996**, *27*, 353–376.
(67) Knözinger, H.; Huber, S. *J. Chem. Soc., Faraday Trans.* **1998**, *94*, 2947–2059.
(68) Zecchina, A.; Scarano, D.; Bordiga, S.; Spoto, G.; Lamberti, C. *Adv. Catal.* **2001**, *46*, 265–397.
(69) Lamberti, C.; Groppo, E.; Spoto, G.; Bordiga, S.; Zecchina, A. *Adv. Catal.* **2007**, *51*, 1–74.

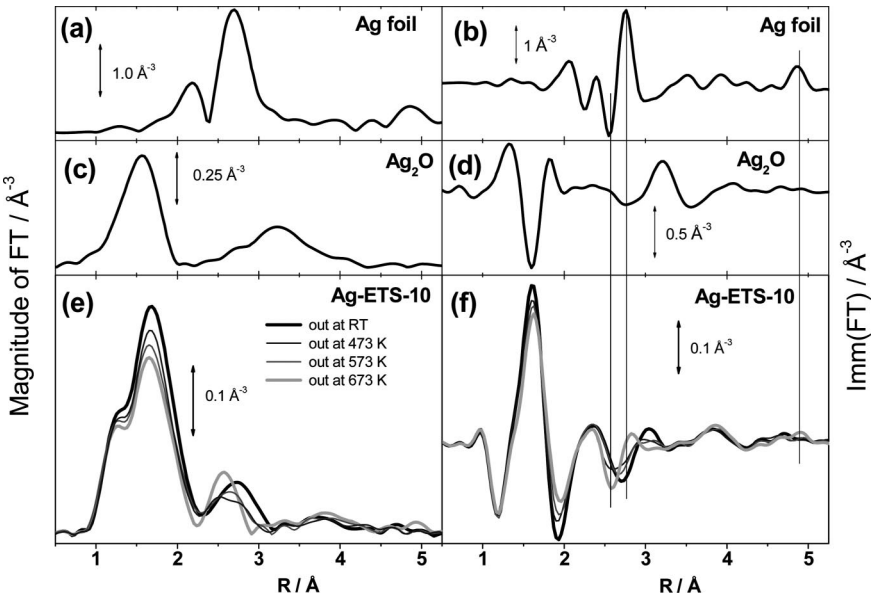

Figure 4. k^2-weighted, phase-uncorrected FT of the EXAFS spectra. (a) Modulus of Ag foil model compound. (b) Like part a for the imaginary part. (c) Modulus of Ag_2O model compound. (d) Like part c for the imaginary part. (e) Modulus of the Ag−ETS-10 sample outgassed at increasing temperatures. (f) Like part e for the imaginary part. Vertical lines in the right panels allow discrimination of features peculiar of the imaginary part of Ag metal.

and UV−vis results).[70−74] In the case of silver-exchanged zeotypes, in fact, an excessive increase of the activation temperature can induce severe reduction of Ag^+ to Ag^0 followed by the formation of Ag_n clusters (see section 4).

At low P_{CO}, a single symmetric band centered at 2180 cm^{-1} is observed (light gray curves in Figure 3a), while no modifications in the ν(OH) region occur (curves not reported in part b). On the basis of comparison with extensive literature data for CO adsorbed on Ag-zeotypes,[70,72,74−77] this band is assigned to the ν(CO) stretching mode of $Ag^+\cdots CO$ adducts formed inside the channels of Ag−ETS-10. It is worth noticing that corresponding wavenumber values for $Ag^+\cdots CO$ adducts formed inside Ag−ZSM-5[70,74,76,77] and Ag−Y[72] systems are 2192−2190 and 2186 cm^{-1}, respectively (i.e., frequencies blue-shifted with respect to the Ag−ETS-10 system of 12−10 and 6 cm^{-1}). This important difference reflects a weaker interaction between the probe molecule (CO) and the cationic site (Ag^+) of Ag−ETS-10. It has been shown that the interaction of CO with isolated Ag^+ cations inside the zeolitic framework is mainly due to electrostatic and σ-donation effects.[74] Consequently, the scale of the frequency shift Ag−ZSM-5 > Ag−Y > Ag−ETS-10 simply reflects the scale of local electric field strength.[78,79] An alternative way to explain a lower ν(CO) value is to hypothesize the formation of $(H_2O)_n$ $Ag^+\cdots CO$ complexes. In fact, Hadjiivanov[76] has shown that upon dosing water vapor on $Ag^+\cdots CO$ complexes previously formed inside Ag−ZSM-5, the C−O stretching frequency red-shifts from 2192 to 2181 cm^{-1}. In our case, however, the formation of mixed $(H_2O)_n$ $Ag^+\cdots CO$ complexes on Ag−ETS-10 activated at 423 K cannot be inferred to explain the observed ν(CO), as spectra collected on Ag−ETS-10 activated at 473 and 573 K show the $Ag^+\cdots CO$ component exactly at the same frequency; see Figure S2 in the Supporting Information. Consequently, the explanation based on the different local electric field strength, previously discussed, holds.

When the pressure increases (dark gray curves in Figure 3a), the band at 2180 cm^{-1} becomes very intense up to saturation, accompanied by the growth of a second peak at 2160 cm^{-1}. The appearance of this second band is accompanied by the consumption of the band at 3735 cm^{-1} (assigned to unperturbed silanols and titanols) and by the formation of a new intense and complex component in the 3550 − 3630 cm^{-1} range (dark gray curves Figure 3b). Consequently, the 2160 cm^{-1} band is assigned to the ν(CO) mode of CO molecules adsorbed on silanols and titanols.[80,81] Finally, further increases of P_{CO} leads to the saturation of the peak at 2160 cm^{-1} and to the growth of a new band centered at 2140 cm^{-1}, easily reversible even at 100 K, due

(70) Bordiga, S.; Lamberti, C.; Turnes Palomino, G.; Geobaldo, F.; Arduino, D.; Zecchina, A. *Microporous Mesoporous Mater.* **1999**, *30*, 129–135.
(71) Bordiga, S.; Turnes Palomino, G.; Arduino, D.; Lamberti, C.; Zecchina, A.; Otero Areán, C. *J. Mol. Catal. A: Chem.* **1999**, *146*, 97–106.
(72) Prestipino, C.; Lamberti, C.; Zecchina, A.; Cresi, S.; Bordiga, S.; Palin, L.; Fitch, A. N.; Perlo, P.; Marra, G. L. *Stud. Surf. Sci. Catal.* **2002**, *142*, 1963–1970.
(73) Lamberti, C.; Prestipino, C.; Bordiga, S.; Fitch, A. N.; Marra, G. L. *Nucl. Instrum. Methods Phys. Res. B* **2003**, *200*, 155–159.
(74) Bolis, V.; Barbaglia, A.; Bordiga, S.; Lamberti, C.; Zecchina, A. *J. Phys. Chem. B* **2004**, *108*, 9970–9983.
(75) Baba, T.; Akinaka, N.; Nomura, M.; Ono, Y. *J. Chem. Soc., Faraday Trans.* **1993**, *89*, 595–599.
(76) Hadjiivanov, K. I. *Microporous Mesoporous Mater.* **1998**, *24*, 41–49.
(77) Kuroda, Y.; Onishi, H.; Mori, T.; Yoshikawa, Y.; Kumashiro, R.; Nagao, M.; Kobayashi, H. *J. Phys. Chem. B* **2002**, *106*, 8976–8987.
(78) Bordiga, S.; Garrone, E.; Lamberti, C.; Zecchina, A.; Otero Areán, C.; Kazansky, V. B.; Kustov, L. M. *J. Chem. Soc., Faraday Trans.* **1994**, *90*, 3367–3372.
(79) Lamberti, C.; Bordiga, S.; Geobaldo, F.; Zecchina, A.; Otero Areán, C. *J. Chem. Phys.* **1995**, *103*, 3158–3165.
(80) Zecchina, A.; Bordiga, S.; Spoto, G.; Scarano, D.; Petrini, G.; Leofanti, G.; Padovan, M.; Otero Areán, C. *J. Chem. Soc., Faraday Trans.* **1992**, *88*, 2959–2969.
(81) Bordiga, S.; Scarano, D.; Spoto, G.; Zecchina, A.; Lamberti, C.; Otero Areán, C. *Vib. Spectrosc.* **1993**, *5*, 69–74.
(82) Bordiga, S.; Escalona Platero, E.; Otero Areán, C.; Lamberti, C.; Zecchina, A. *J. Catal.* **1992**, *137*, 179–185.
(83) Zecchina, A.; Bordiga, S.; Lamberti, C.; Spoto, G.; Carnelli, L.; Otero Areán, C. *J. Phys. Chem.* **1994**, *98*, 9577–9582.

to the liquidlike CO phase formed inside the zeolite channels.[81−83]

3.3. Local Environment of Ag^+ Species Probed by EXAFS. The local environment of Ag species has been investigated by EXAFS spectroscopy. The k^2-weighted, phase-uncorrected FT of the EXAFS spectrum of Ag−ETS-10 outgassed at RT is reported in Figure 4e and f, bold black curves. The spectrum is characterized by two main components centered around 1.7 and 2.7 Å (without phase correction). The former is due to Ag−O contributions that are optimized at 2.33 ± 0.02 Å, a value typical for the distance between silver cations and oxygen framework atoms of zeolitic materials.[70−74,84] The optimized coordination number is $N = 3.0 \pm 0.4$ and has to be considered as an average value, as different cationic sites have been found in ETS-10.[6,11,20,85] It is of interest to note that, although contributing almost in the same *R*-range to the magnitude of the FT (see Figure 4c and e), the Ag−O signals of Ag_2O model compound and of Ag−ETS-10 outgassed at RT are completely out of phase (minimum vs maximum of the imaginary part at $R = 1.62$ Å, Figure 4d and f). This peculiarity reflects the fact that the corresponding $k^2\chi(k)$ functions (not reported for brevity) exhibit a phase difference close to π in a very large k interval, due to the significant difference in the Ag−O distance: 2.00 Å in Ag_2O and 2.33 ± 0.02 Å in Ag−ETS-10.

Coming to the component at 2.7 Å, it appears in the same *R*-interval of the Ag−Ag contribution in silver metal (see Figure 4a). However, the presence of clustered Ag^0 particles in Ag−ETS-10 outgassed at RT has to be discarded on the basis of an inspection of the imaginary parts; compare parts b and f of Figure 4. By following the vertical line drawn at $R = 2.75$ Å, it is evident that it corresponds to a maximum of the imaginary part of the silver foil and to a minimum of that of Ag−ETS-10. The component at 2.7 Å is consequently assigned to a combination of both Ag−Ti and Ag−Si, contribution from the framework atoms, and of Ag−Na and Ag−K contribution from adjacent, nonexchanged Na^+ and K^+ counterions (Figure 1b). Due to the complexity of this signal, no simulation of this component has been attempted. Note that the situation is further complicated by the presence of several possible cationic sites for Ag^+ and by an additional higher shell heterogeneity induced by the partial Ag-exchange nature of the sample. From the EXAFS investigation of Ag−ETS-10 outgassed at RT, it is concluded that all silver species present in the sample are in the form of dispersed Ag^+ ions and that no Ag^0 clustering is present.

The successive sections are devoted to developing methods able to tune the nuclearity of Ag nanoclusters formed inside ETS-10 channels or on the external surface of the zeolite crystals. First, we will discuss the standard reduction processes: thermal reduction in vacuo at increasing temperatures (section 4) and H_2-reduction at increasing temperatures (section 5). Finally, the photoreactivity of the material has been tested (section 6). In sections 5 and 6, the reversibility of the process has been tested performing thermal treatments in O_2 atmosphere at increasing temperatures and photooxidation treatments in air using visible light, respectively.

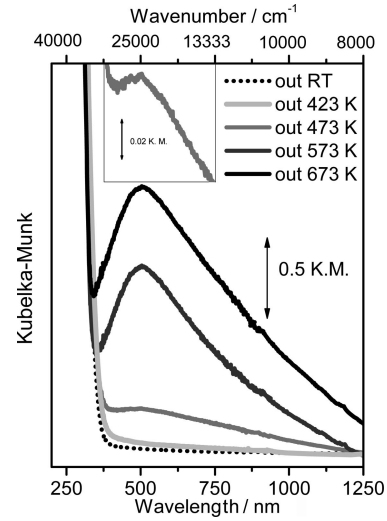

Figure 5. UV−vis spectra of Ag−ETS-10 outgassed at increasing temperatures. See legend. The inset reports a magnification, in the 375−750 nm range, of the spectrum obtained on the sample activated at 473 K, allowing appreciation of the maximum of the absorption at 500 nm (25 000 cm^{-1}).

4. Activation of Ag−ETS-10 at Increasing Temperatures

4.1. EXAFS Study. The EXAFS study reported in Figure 4e and f indicates that the average local environment of silver cations is modified upon increasing the temperature of the activation treatment, up to 673 K. In particular, the contribution centered around 1.7 Å loses intensity progressively, while the component at higher *R* is progressively modified in both modulus shape and maximum position (moving from 2.7 to 2.55 Å) and in modulation of the imaginary part. In the 2.3−3.0 Å region, the imaginary part of the Ag−ETS-10 evacuated at 673 K is in phase with that of the Ag−Ag first shell contribution in the Ag metal model compound (Figure 4b): minimum at 2.55 Å and maximum at 2.75 Å; see vertical lines. From this EXAFS study, it can be concluded that a minor fraction of Ag^+ is progressively reduced to Ag^0, which aggregates to form small Ag metal nanoclusters.

4.2. UV−vis Study. Figure 5 reports the UV−vis spectra of Ag−ETS-10 outgassed under dynamic vacuum at different temperatures. The spectra evolution corresponds to color changes of the sample from white (RT) through white/pale gray (423 K), gray (473 K), dark gray (573 K), to nearly black (673 K). Concerning Ag−ETS-10 outgassed at RT, as discussed in section 3.1, the spectrum is dominated by the presence of an intense band starting at about 340 nm and assigned to the transition from valence to conduction band in −O−Ti−O−Ti− quantum wires.[7,14,26,27] Note that in this case the ion exchange causes a significant broadening of the adsorption edge of ETS-10; see Figure 2. No significant differences are observed upon activation at 423 K: only a negligible tail in the 400−500 nm range is observed. This evidence implies that Ag−ETS-10 sample

(84) Suzuki, Y.; Matsumoto, N.; Ainai, T.; Miyanaga, T.; Hoshino, H. *Polyhedron* **2005**, *24*, 685–691.
(85) Grillo, M. E.; Carrazza, J. *J. Phys. Chem.* **1996**, *100*, 12261–12264.

activated at 423 K still contains almost only isolated Ag^+ species and that the IR spectroscopy of adsorbed CO reported in Figure 3 is quite representative of the available surface sites of the as-exchanged sample. As for sample activated at 473 K, it is possible to observe the presence of a clear wide band starting from 410 nm and extending up to 1200 nm, i.e. covering all the visible and near-infrared (NIR) regions. The maximum of this band is centered at 500 nm, as evidenced in the inset. This component becomes significantly more pronounced in the samples activated at 573 and 673 K and is interpreted as the plasmon resonance of silver nanoparticles,[36,38] that originates from the collective oscillations of conduction electrons.

Note that, even after activation at 573 K, the largely predominant silver species are still isolated Ag^+ (vide supra the EXAFS study in section 4.1, Figure 4, and see the FTIR study reported in the Supporting Information, Figure S2). This means that only a small fraction of silver is in the clustered form and that the intense UV−vis band centered at ~500 nm reflects the huge extinction coefficient of the silver nanoparticles.[36,38] In fact, the combined measurements of extinction, scattering, and absorption cross sections and efficiencies of colloidal silver nanoparticles in water indicate that particles interact with light up to 10 times stronger than the geometric cross section suggests.[36]

In principle, the maximum plasmon resonance can be correlated to the nanoparticle dimension. Evanoff and Chumanov investigated Ag colloidal nanoparticles characterized by a narrow particle size distribution (16 different samples have been carefully prepared and measured via systematic scanning electron microscopy (SEM) investigation), showing that the plasmon resonance of colloidal silver nanoparticles in water with an increasing average size ranging from 29 to 136 nm moves from ≈420 to ≈580 nm.[36,86] Unfortunately, we cannot use this systematic calibration to infer, from the spectra reported in Figure 5, the average particle size of the Ag nanoparticles formed in Ag−ETS-10, because many other factors like the shape of the particle, dielectric constant of the surrounding medium, and applied voltage influence significantly the profile and the position of the plasmon band.[38,87,88] In particular, the local electromagnetic field that extends beyond the physical boundaries of the particles is defined as that providing "feedback" between the local environment and the electron oscillations in a particle.[87] This point has a relevant effect in our case, as local electric fields as high as volts per nanometer (10^9 V m^{-1}) are present at cationic sites in zeolites.[79,83] Consequently, no quantitative results can be easily extracted from the spectra reported in this work. In particular, the huge amplitude of the plasmon absorption extending from the visible to NIR region (400−1200 nm) is probably reflecting the presence of silver nanoparticles with a broad size distribution, with diameters ranging from less than 1 nm, characteristic of particles inside the channel network whose growth is blocked from the cavities, up to much larger values, belonging to aggregates formed on the external surface of ETS-10 where their growth does not experience steric impedance. Unfortunately, also tunneling electron microscopy (TEM) could not be used to measure the particle size distribution in Ag−ETS-10 samples as the high vacuum, first, and the electron beam, more efficiently, were external causes of silver reduction and aggregation.

The evolution of the 500 nm band in the UV−vis spectra upon increasing the activation temperature (see Figure 5) qualitatively mirrors the evolution of the Ag−Ag contribution observed by EXAFS (see Figure 4). On this basis, it is concluded that both UV−vis DRS and EXAFS are very useful techniques to follow the Ag cluster formation.

5. H_2-Reduction/O_2-Oxidation: An Almost Reversible Red−Ox Behavior

In order to try to achieve a higher fraction of reduced silver, ETS-10 was reduced by molecular hydrogen at increasing temperatures. The process of the H_2-reduction of Ag^+ ions in zeotype has been extensively studied with volumetric methods as well as many spectroscopic techniques such as IR spectroscopy.[75,89] The hydrogen reduction of Ag^+ ions in zeolite to the metallic state occurs according to the following equation:

$$n\mathrm{T{-}O^{-}Ag^{+}{-}T} + {}^{1}/_{2}n\mathrm{H_2} \rightarrow n\mathrm{Ag^0} + n\mathrm{T{-}O^{-}H^{+}{-}T} \quad (1)$$

where $T-O^-Ag^+-T$ denotes the oxygen anion of the zeolitic framework, whose charge is balanced by the Ag^+ cation (T = Si or Al in zeolites and T = Si or Ti in ETS-10) and where $T-O^-H^+-T$ represents the Brønsted group. This type of reaction is partially reversible, because it has been observed that by exposing the system to an oxygen atmosphere Ag^+ ions are restored via the following equation:

$$n\mathrm{Ag^0} + {}^{1}/_{4}n\mathrm{O_2} + n\mathrm{T{-}O^{-}H^{+}{-}T} \rightarrow n\mathrm{T{-}O^{-}Ag^{+}{-}T} + {}^{1}/_{2}n\mathrm{H_2O} \quad (2)$$

The degree of reversibility is strictly associated with cluster dimension; clusters with greater dimension are more difficult to oxidize, and an increase of temperature is needed. Both reactions 1 and 2 have been followed in situ by IR spectroscopy of adsorbed CO, EXAFS, and UV−vis spectroscopies. After each reduction−oxidation process, the crystallinity of the samples has been checked by XRD. All measured patterns (not reported for sake of brevity) do not show significant modification, reflecting that the crystallinity of the material is preserved during the red−ox cycle described in reactions 1 and 2.

5.1. H_2 Reduction. The effect of reaction 1, carried out at 423 K, is evident by comparing the IR spectra of Ag−ETS-10 activated in vacuum at 423 K (gray curve in Figure 6b, vertically translated for clarity) and that of the sample reduced in H_2 at the same temperature (dotted black

(86) Evanoff, D. D.; Chumanov, G. *J. Phys. Chem. B* **2004**, *108*, 13948–13956.
(87) Evanoff, D. D.; White, R. L.; Chumanov, G. *J. Phys. Chem. B* **2004**, *108*, 1522–1524.
(88) Evanoff, D. D.; Zimmerman, P.; Chumanov, G. *Adv. Mater.* **2005**, *17*, 1905–1908.
(89) Cvjeticanin, N. D.; Petranovic, N. A. *Zeolites* **1994**, *14*, 35–41.

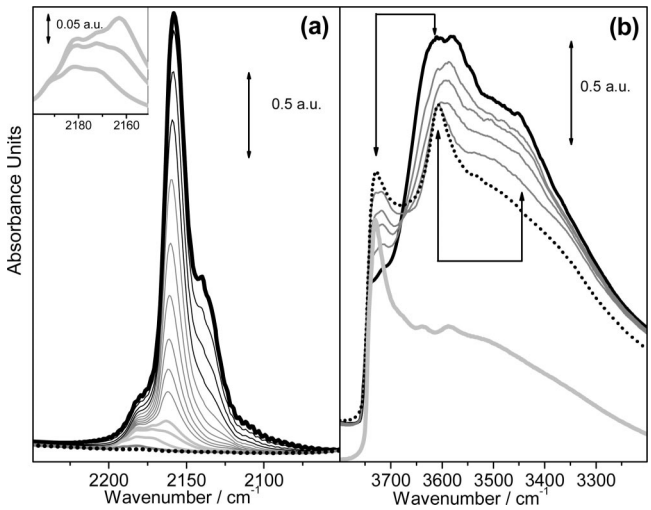

Figure 6. Evolution of IR spectra of CO adsorbed at 100 K on Ag−ETS-10 H_2-reduced at 423 K (dotted black spectrum), as a function of increasing equilibrium pressure (up to P_{CO} = 50 Torr, black bold spectrum). Gray thin spectra refer to intermediate P_{CO} values. Part a reports background subtracted spectra and refers to the ν(CO) stretching region. The same color code is used as in Figure 2. The three spectra collected at the lowest P_{CO} are reported in the inset with an enlarged ordinate scale. Part b refers to the ν(OH) stretching region. Also, the spectrum of Ag−ETS-10 outgassed at 423 K down to 10^{-4} Torr (light gray curve) is reported for comparison (vertically shifted). The arrows evidence the shifts of the ν(OH) bands due to CO adsorption.

spectra in Figure 6b). The appearance upon reduction of the T−O$^-$H$^+$−T Brønsted groups is evident by looking at the intense and well-defined peak at about 3608 cm^{-1}, equivalent to the band observed in the H−ETS-10 sample (see light gray curve in Figure 2b).

In the same figure, the effect of CO dosage at 100 K on H_2-reduced Ag−ETS-10 is also reported (increasing P_{CO} from 10^{-4} to 50 Torr), in both the C−O and O−H stretching regions (part a and b, respectively). CO probes clearly the great difference in the available surface site population of the Ag−ETS-10 channels upon reduction in H_2 at 423 K. The component at 2180 cm^{-1}, ascribed to Ag$^+$···CO complexes, is depressed by an order of magnitude in intensity, the component at 2160 cm^{-1}, due to OH···CO adducts, dominates now the spectra, and the component at 2140 cm^{-1}, due to liquidlike CO molecules filling the zeolitic channels, loses more than 2/3 of its intensity; compare Figure 6a with Figure 3a. This IR experiment testifies that almost 90% of Ag$^+$ counterions have been subjected to the reduction described in reaction 1. About the aggregation type of silver, nothing can be inferred from this IR study because CO does not interact with Ag^0 atoms at the surface of the silver clusters at the investigated P_{CO} and temperature. EXAFS and UV−vis will be used for this purpose. In an indirect way, we can just observe that the significant decrease of the liquidlike component (at the same temperature and P_{CO}) is typical of a reduction of the available pore volume, probably occluded by the formation of Ag^0 nanoclusters. It is worth noting that the C−O stretching frequency of carbon monoxide adsorbed on silanols or titanols (Figure 3a) and on Brønsted sites (Figure 6a) inside the ETS-10 framework is almost equivalent. We could conclude that CO is unable to distinguish between the two different type of sites, which is a consequence of the moderate weak acidic nature of Brønsted sites inside the protonic form of ETS-10. This fact is confirmed by an inspection of the evolution of the spectra in the O−H stretching region (Figure 6b), where CO adsorption is causing the erosion of the band at 3608 cm^{-1} (ascribed to Si−O$^-$H$^+$−Ti acidic sites) and the growth of a new band at 3450 cm^{-1}. This wavenumber shift of $\Delta\tilde{\nu}$(OH) = −158 cm^{-1} gives an estimation of the low acidity of these groups: the $\Delta\tilde{\nu}$(OH) observed for a strong acid Si−O$^-$H$^+$−Al sites in protonic zeolites such as H−ZSM-5,[80] H−β,[90] or H−MORD[91] is −335, −319, and −291 cm^{-1}, respectively corresponding to $\tilde{\nu}$(CO) values of 2178, 2177, and 2172 cm^{-1}. At higher P_{CO}, also the component at 3730 cm^{-1}, due to titanols and silanols, is eroded resulting in the formation of a new band at 3618 cm^{-1}, due to the formation of hydrogen-bonded T−OH···CO complexes.

Information on the Ag^0 nanoparticles formed upon H_2 reduction comes from the EXAFS and UV−vis spectra reported in Figure 7, parts a and b respectively. Reduction at 323 K (bold light gray curve) results in a partial reduction of silver species: the EXAFS spectrum is still dominated by the Ag−O contribution and a small peak in the Ag−Ag region appears.[92] An important fraction of well defined Ag^0 nanoparticles starts to be formed upon reduction at 373 K, as clearly seen in the EXAFS spectrum (gray line), where the higher shell contributions in the 4−6 Å region start to be clearly visible. However, a fraction of isolated Ag$^+$ species is still present. According to the EXAFS datum, an almost complete reduction is achieved for the sample reduced at 423 K (the same temperature adopted in the IR study; see Figure 6), dark gray curves. The UV−vis spectrum of this last sample shows an absorption different from those observed in the case of the sample activated at 573 K (scattered light gray curve, multiplied by a 3.1 factor) and reduced in H_2 at 423 K. While the position of the maximum is almost unchanged, the much larger low energy tail of the band observed for the H_2-reduced sample is evident. This asymmetry reflects a broader particle size distribution with an increased fraction of large particles.[36,38] Both EXAFS and UV−vis spectroscopies indicate that the clustering is more effective for the sample H_2-reduced at 573 K.

From the set of EXAFS spectra reported in Figure 7a, the intensity of the first shell Ag−Ag signal cannot be used to safely estimate the average particle size as it strongly correlates with the fraction of oxidized/reduced silver. The latter can not be determined as we do not have a specific model for the Ag−O contribution of the fraction of isolated Ag$^+$ species. As discussed in section 3.3, the Ag−O signal of the sample outgassed at RT results from the combination of a different local environment of isolated Ag$^+$ species. As we expect that different Ag$^+$ sites will have a different

(90) Pazé, C.; Bordiga, S.; Lamberti, C.; Salvalaggio, M.; Zecchina, A.; Bellussi, G. *J. Phys. Chem. B* **1997**, *101*, 4740–4751.
(91) Bordiga, S.; Lamberti, C.; Geobaldo, F.; Zecchina, A.; Turnes Palomino, G.; Otero Areán, C. *Langmuir* **1995**, *11*, 527–533.
(92) The corresponding UV−vis spectrum (not reported) shows, as expected, a plasmon resonance of weak intensity but characterized by an anomalous shape, probably related to the variation of the local dielectric constant around Ag nanoparticles due to the presence of a significant fraction of water that has not been removed from the sample owing to the low activation temperature and to the large amount of sample needed to perform a UV−vis DRS spectrum.

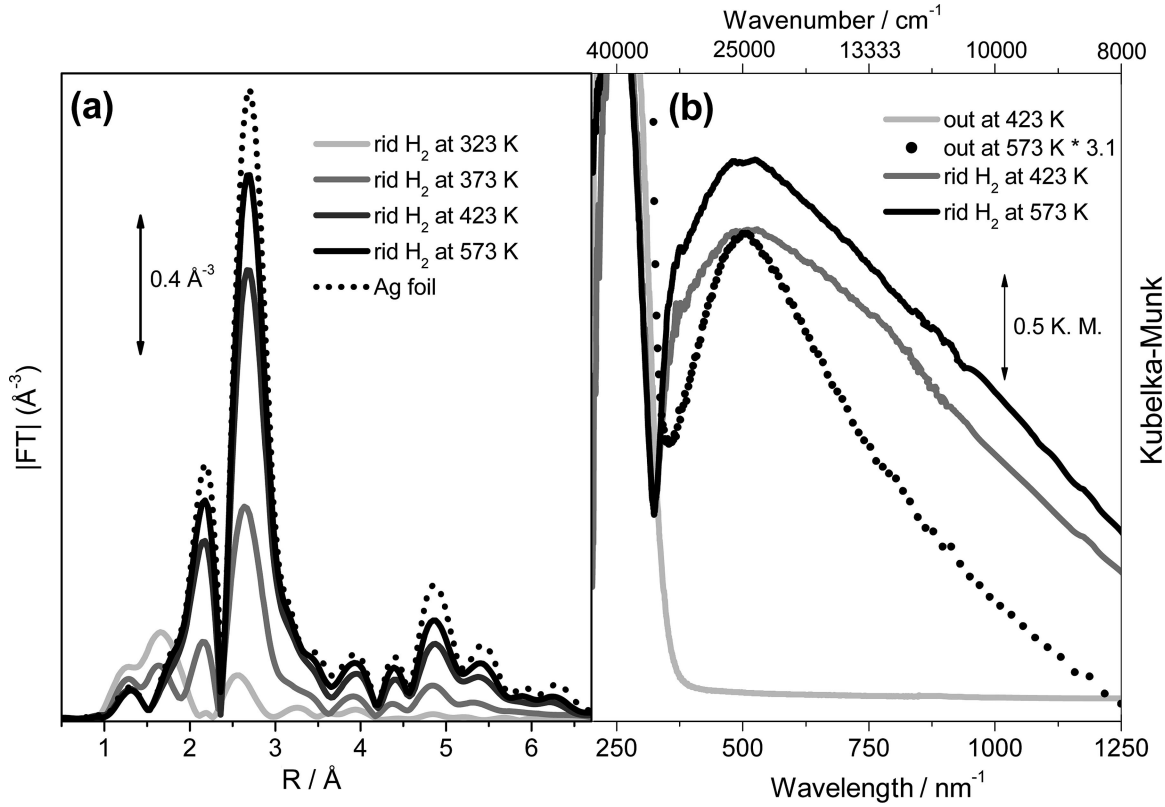

Figure 7. Effect of H_2 reduction at increasing temperatures on the k^2-weighted, phase-uncorrected FT of the EXAFS spectra and on the UV−vis spectra, parts a and b respectively. For sake of comparison, the spectrum of Ag foil reference compound is included in part a, while (from Figure 5) those of the Ag−ETS-10 samples activated at 423 and 573 K (the latter multiplied by a factor 3.1 to match the intensity of the plasmon peak of the sample reduced in H_2 at 423 K) are added in part b.

reducibility, we do not have a safe model to estimate the fraction of cationic silver. Assuming a complete reduction for the sample reduced at 573 K, from a first shell EXAFS analysis, a coordination number of $N = 11.2 \pm 0.6$ is obtained ($N = 12.0$ for the bulk phase), suggesting an average particle size larger than ≈80 Å. This value demonstrates that a fraction of the Ag species has migrated outside the zeolitic channels. Table S1 of the Supporting Information reports the results of the first shell EXAFS data analysis of the samples reduced in H_2 at 423 and 573 K.

5.2. O_2 Reoxidation. H_2-reduced samples have been subjected to a progressive oxidation treatments in O_2 atmosphere at increasing temperatures to check the reversibility of the reduction and clustering effect described in section 5.1. IR spectroscopy performed on H_2-reduced 423 K Ag−ETS-10 sample before and after oxidation at 423 K (Figure 8b) shows the almost complete erosion of the well defined peak at about 3608 cm^{-1} due to T−O^-H^+−T Brønsted groups. This demonstrates that the charge balancing counterions are no more the protons. IR spectroscopy of adsorbed CO (Figure 8a) shows that this role is played again by Ag^+ cations, according to reaction 2. In fact, the component at 2180 cm^{-1}, ascribed to $Ag^+\cdots CO$ complexes, which almost disappeared in the H_2-reduced samples (see Figure 6a), is restored again and dominates the spectra in Figure 8b. The component at 2160 cm^{-1} (ascribed to OH···CO adducts) is decreased in intensity but does not disappear, due to the presence of surface titanols and silanols. Finally, the CO liquidlike component at 2140 cm^{-1} is still

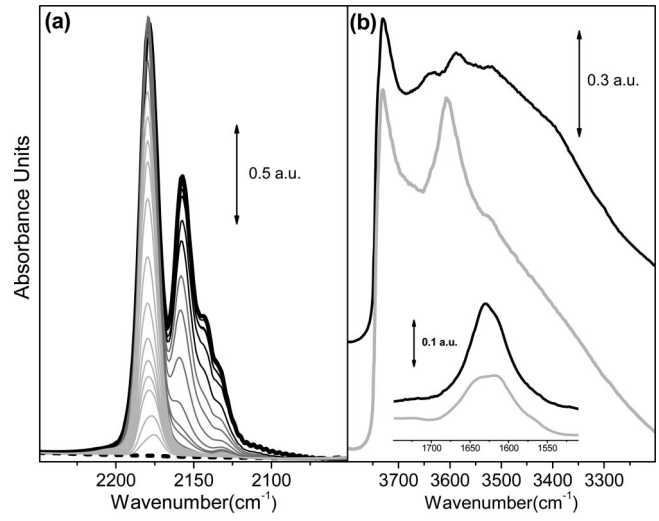

Figure 8. (a) Evolution of IR spectra in the C−O stretching region, of CO adsorbed, at 100 K and increasing P_{CO} (up to P_{CO} = 50 Torr, black bold spectrum) on Ag−ETS-10 reduced in H_2 at 423 K and successively oxidized in O_2 at the same temperature (dotted black spectrum). Gray thin spectra refer to intermediate P_{CO} values. The same color code is used as in Figure 2. (b) IR spectra in the ν(OH) region of Ag−ETS-10 reduced in H_2 at 423 K (gray curve, vertically shifted for clarity) and of the same sample subjected to a successive oxidation treatment in O_2 at 423 K (black curve). The inset reports the same spectra in the δ(OH) region.

as weak as in the H_2-reduced samples (see Figure 6a) and does not recover the intensity observed before reduction (see Figure 3a). This overall behavior suggests that, while the high majority of silver species is back-converted into isolated Ag^+ cations, a minority fraction of high nuclearity Ag^0 clusters is still present and blocks an important fraction of

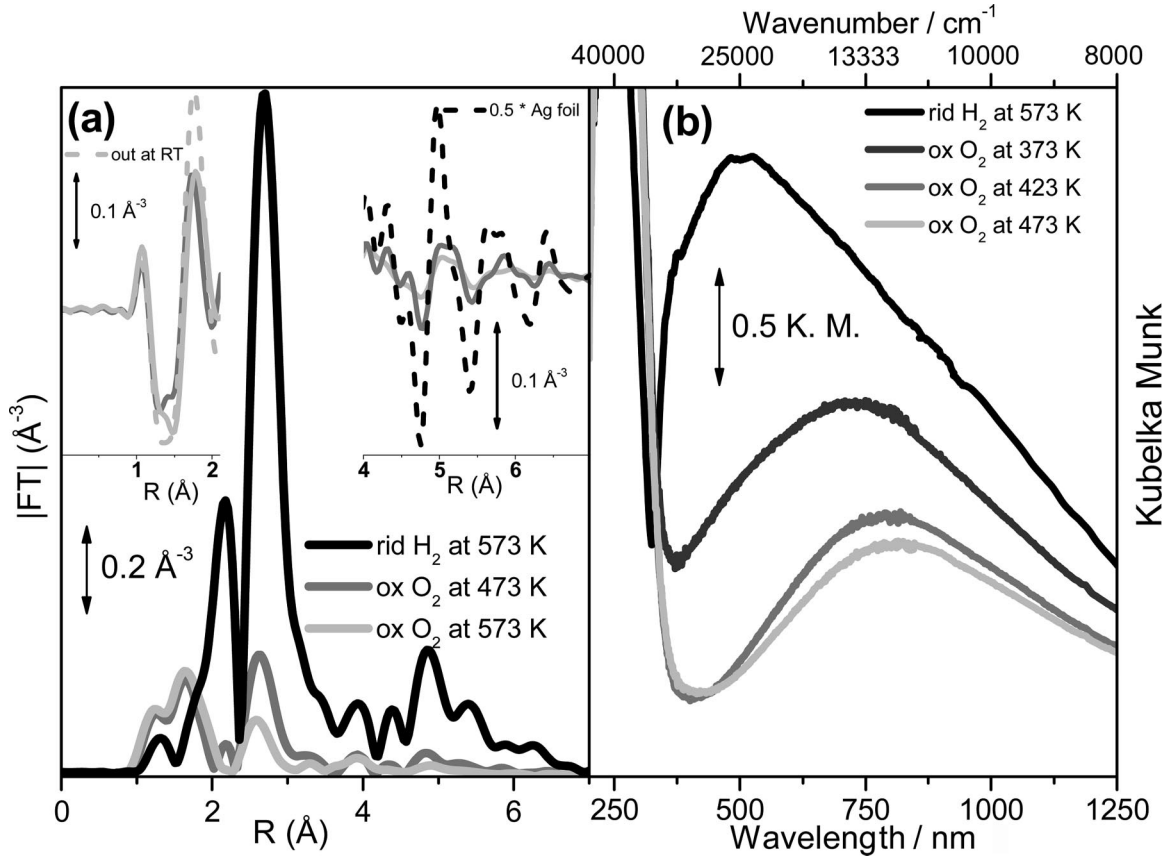

Figure 9. (a) Effect on the EXAFS spectra of O_2 oxidation in the atmosphere at increasing temperatures (473 and 573 K, gray curves) of the Ag−ETS-10 sample previously reduced in H_2 at 573 K (black spectrum). The left inset reports, in the Ag−O contribution range, the imaginary parts of the reoxidized samples (same lines) together with that of the Ag−ETS-10 activated at RT and considered as a model of 100% isolated Ag^+ species (dashed gray line). The right inset reports, in the higher shells Ag−Ag contribution range, the imaginary parts of the reoxidized samples (same lines) together with that of the Ag foil model compound (black dashed line) divided by a factor of two. (b) Effect on the UV−vis spectra of O_2 oxidation at increasing temperatures (373, 423, and 473 K, full gray curves) of the Ag−ETS-10 previously reduced in H_2 at 573 K (black spectrum).

the ETS-10 channels, that cannot be filled by CO at high P_{CO} conditions. The evolution of the IR spectra in the O−H stretching region, upon increasing P_{CO}, does not differ significantly from the set of spectra obtained before H_2 reduction (see Figure 3b) and are consequently not reported for brevity.

EXAFS and UV−vis spectroscopies have been used to investigate the evolution of clustered Ag^0 nanoparticles, as they are not detected by IR spectroscopy of adsorbed CO. The fact that most of the aggregated Ag^0 species are reversibly converted into isolated Ag^+ species, as indirectly suggested by the almost complete recovery of the IR band of $Ag^+\cdots CO$ complexes at 2180 cm^{-1}, is directly confirmed by the EXAFS and UV−vis spectra reported in parts a and b of Figure 9, respectively. The Ag−Ag first shell contribution in the 2−3 Å range, dominating the FT of the EXAFS spectrum of the Ag−ETS-10 sample reduced in H_2 at 573 K, loses about 80 and 90% of its intensity upon reoxidation at 473 and 573 K, respectively. Although very small in percentage, the remaining fraction of aggregated Ag^0 species is in form of relatively large metal particles, as shown by the presence of the higher shell contributions in the 4−6 Å range, whose imaginary parts (see right inset) are in phase with that of the Ag foil model compound. The loss of the contribution of aggregated Ag^0 species is balanced by the recovery of the Ag−O first shell signal in the 1−2 Å range. Also in this case, the corresponding imaginary parts are in perfect phase with the imaginary part of the Ag−ETS-10 sample activated at RT that has been proved to contain only isolated Ag^+ species (see left inset). Coming to the intensity of the Ag−O first shell signal, it is recovered by the reoxidation process by a factor close to 0.75 with respect to the intensity of the signal measured for Ag−ETS-10 sample activated at RT.

UV−vis spectra clearly show that, upon increasing the temperature of the O_2 reoxidation process, the plasmon resonance peak is significantly decreased in intensity and red-shifted in frequency of the maximum; see Figure 9b. The intensity loss reflects the decrease in the fraction of aggregated Ag^0 nanoparticles already observed by EXAFS. The shift of the maximum, from 500 nm (H_2-reduced sample) up to 720, 800, and 820 nm for samples reoxidized at 373, 423, and 473 K, respectively, reflects an important modification of the particle size distribution, confirming that the smaller nanoparticles, characterized by plasmon resonances at lower wavelengths,[36,38] are, by far, preferentially disaggregated during the O_2 treatment. The optical investigation is thus in qualitative agreement with the EXAFS study, showing that the fraction of silver that resists the reoxidation process is characterized by large particles (see right inset in Figure 9a) and with the IR study, showing that an important fraction of the ETS-10 channels is still obstructed by Ag metal particles (Figure 8a).

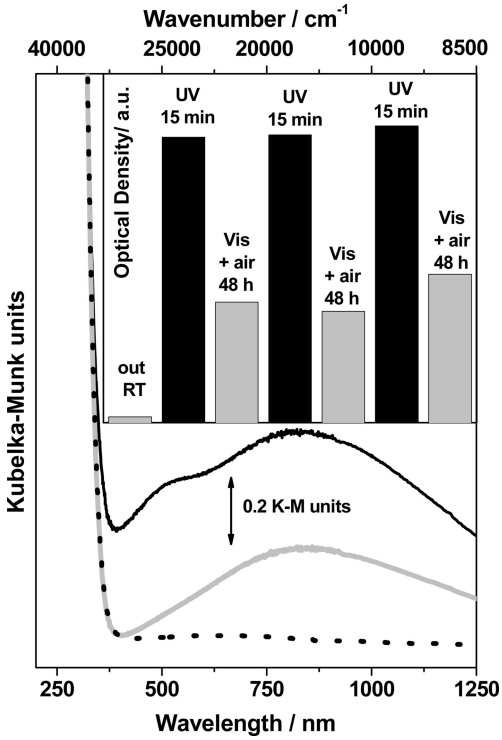

Figure 10. Effect on the UV−vis spectrum of Ag−ETS-10 (dotted black line) of irradiation with UV photons, in air for 15 min, (black full line) and of successive irradiation with solar photons, in an air atmosphere for 48 h, (gray full line). The inset reports the evolution of the integrated band in the 500−1250 nm range upon several successive alternated UV-reduction/vis-oxidation treatments.

6. UV-Photoreduction and Vis-Photo-oxidation of Ag−ETS-10: A Highly Reversible Process

In order to prove the photoreactivity of Ag−ETS-10, we have investigated the effect that an UV-irradiation has on the sample. It is in fact known that Ag^+ counterions can be reduced and aggregated upon exposure to UV light.[47,93,94] Figure 10 reports the effect of 15 min of UV irradiation on the Ag−ETS-10 sample, as monitored by UV−vis spectroscopy (compare full and dotted black lines). UV-irradiation causes the appearance of a broad absorption covering almost the whole visible and NIR region of the electromagnetic spectrum and exhibiting two marked components around 20 000 cm^{-1} (500 nm) and 12 000 cm^{-1} (830 nm). This is clear evidence of the aggregation of isolated Ag^+ ions into Ag^0 clusters characterized by a bimodal size distribution of small and large dimension, respectively.

Moreover, this process is almost reversible, as prolonged illumination (48 h) with visible light in air causes an important decrease of the absorption in the visible region; see the gray full line in Figure 10. The component around 20 000 cm^{-1} (500 nm) is totally eroded by the visible light treatment, while only a small relative fraction of the component at 12 000 cm^{-1} (830 nm) survives. This testifies to a complete vis-photoassisted disgregation of the small metal clusters having a plasmon resonance around 500 nm and an important disgregation of the larger clusters absorbing at larger wavelength. This photoassisted red−ox behavior can be repeated several times, as reported in the inset of Figure 10. Note that the fraction of non-re-oxidized silver is always almost the same, indicating the exception made for this small fraction of large clusters (probably formed in the first UV-treatment); the remaining fraction of silver species are able to aggregate upon brief UV irradiation and are able to be fully disaggregated and reoxidized after prolonged vis-irradiation.

7. Conclusions

Combining UV−vis, Ag K-edge EXAFS, and FTIR spectroscopy of adsorbed CO we have been able to monitor the evolution of the silver aggregation in Ag−ETS-10 along different reduction−oxidation treatments. In particular, we succeed in shifting the ETS-10 light absorption down to the visible region of the electromagnetic spectrum by applying thermal-, chemical-, and UV-photo-treatments on Ag−ETS-10. In such ways, we tune, in a controlled, progressive, and almost reversible manner, the aggregation of isolated Ag^+ counterions into metal nanoclusters of increasing nuclearity. This guarantees the control of the frequency of silver nanoparticle plasmon resonance and thus the light absorption properties of the obtained material. The findings may be relevant for other related titanosilicate molecular sieves like, e.g., ETS-4.[20,32,95−97]

Acknowledgment. This research has been partially supported by the NanoMat project (cofinanced by Regione Piemonte). EXAFS experiments have been performed at BM29 of the ESRF within the frame of the long-term project CH-1700. The support of the ESRF facility, in particular the Chemistry Laboratory (Dr. Müller), and the whole staff of the BM29 beamline are gratefully acknowledged.

Supporting Information Available: FT of the EXAFS signal of silver metal as a function of the different interval in *k*-space, first shell EXAFS data analysis on the Ag−ETS-10 samples reduced in H_2 atmosphere at 423 and 573 K, and the IR spectra of CO dosed at liquid nitrogen temperature on Ag−ETS-10 thermally activated at 473 and 573 K. This material is available free of charge via the Internet at http://pubs.acs.org.

CM803216K

(93) Hidaka, H.; Honjo, H.; Horikoshi, S.; Serpone, N. *Sens. Actuator B: Chem.* **2007**, *123*, 822–828.
(94) Kometani, N.; Kaneko, M.; Morita, T.; Yonezawa, Y. *Colloid Surf. A: Physicochem. Eng. Asp.* **2008**, *321*, 301–307.
(95) Kuznicki, S. M.; Bell, V. A.; Nair, S.; Hillhouse, H. W.; Jacubinas, R. M.; Braunbarth, C. M.; Toby, B. H.; Tsapatsis, M. *Nature* **2001**, *412*, 720–724.
(96) Nair, S.; Jeong, H. K.; Chandrasekaran, A.; Braunbarth, C. M.; Tsapatsis, M.; Kuznicki, S. M. *Chem. Mater.* **2001**, *13*, 4247–4254.
(97) Cruciani, G.; De Luca, P.; Nastro, A.; Pattison, P. *Microporous Mesoporous Mater.* **1998**, *21*, 143–153.